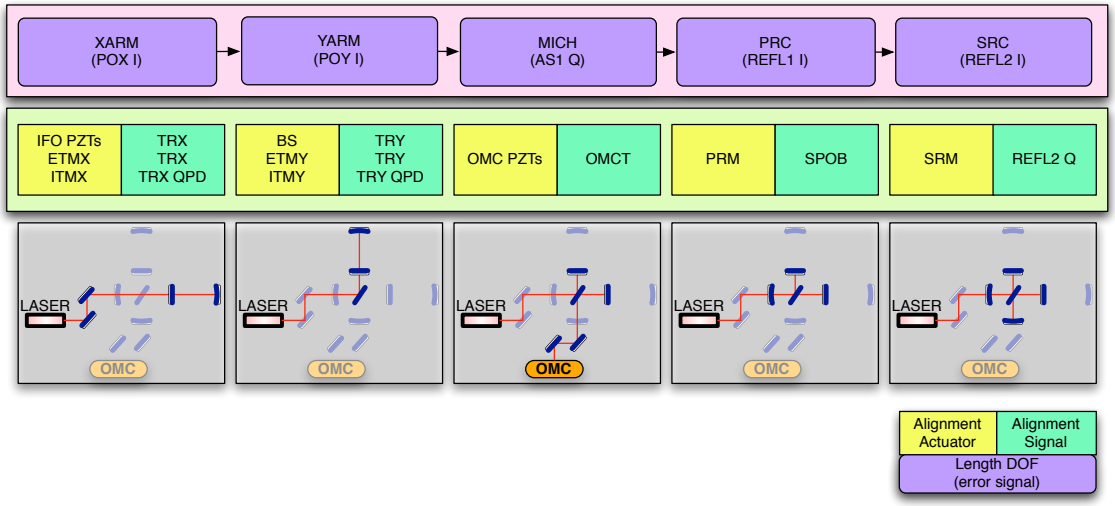

Figure 3.4: Signals and DOFs for bootstrapping the alignment.

3.5.2 The Lock Acquisition Procedure

The lock acquisition procedure developed for the 40 m detuned RSE interferometer will form the basis of the lock acquisition procedure for Advanced LIGO (see [**?**]), and is presented in detail in this thesis for the first time. The basic scheme of the procedure is to first bring the interferometer into a controlled state at a location in phase space which may not be the final operating point, but can be smoothly connected via a known path (each point of which has useful control signals for all DOFs) to the operating point. The definitions of the DOFs can be seen in Figure 2.8. This procedure is shown graphically in Figure 3.10. The first demonstration of this approach was developed in the summer and fall of 2005 and briefly reported in [14]. This approach differs from that taken in Initial LIGO, which essentially sought to go directly from an uncontrolled state to the operating point [11].

Step A: Acquire lock

The first step is to bring the interferometer under control; here the interferometer goes from a globally uncontrolled state (the local control systems are always operational) to a globally controlled state. There are five DOFs to be controlled, each with an error signal as denoted in Table 3.1. Each respec-

tive loop is controlled by a single error signal, and the output of each loop is switched on/off by a trigger. Thus, at this stage, each loop is essentially independent (although MICH and PRC are triggered by the same signal). The typical order of acquisition of these five DOFs can be seen in Figure 3.10 to be (MICH/PRC, SRC, X/Y)—thus, typically the DRMI locks followed by the two ARMs, which lock individually. The three short DOFs (MICH, PRCL, SRCL) are locked at their operating point. The two ARMs are locked off-resonance (using the offset locking technique described in 3.3.3), by the same amount, each somewhat longer than nominal.

Note that none of the signals listed in Table 3.1 are the same as the signals listed in Table 2.1, which are used at the operating point. The initial signals were chosen for their independence of other DOFs, the existence of easily characterized and useful trigger signals, and the ability to easily bootstrap them. In the current implementation, this first stage is statistical in nature, with a non-deterministic period of waiting before all five DOFs can be brought under control. The distribution of times to wait for this stage to be completed is shown in Figure 3.5. Lock wait times which are longer than 15 minutes are excluded from the data. Methods which are more deterministic in nature are currently being studied at the 40 m and are discussed in 3.6.

Step B: Hand off control signals for short DOFs

Once all 5 DOFs of the interferometer are being actively controlled using the signals in table 3.1, the sensing of the short DOFs is handed off to the signals shown in table 3.2. These signal transitions are done digitally, enabling a smooth wipe. The gains of these sDOF loops are ramped up and low-frequency boosts are engaged.

Step C: $X_{DC} + Y_{DC}$ to $DARM_{DC} + CARM_{DC}$

Once the short DOFs are stably controlled, control of the arm cavities is switched from separately sensed and controlled lengths to the common and differential lengths (CARM and DARM). This decomposition more closely

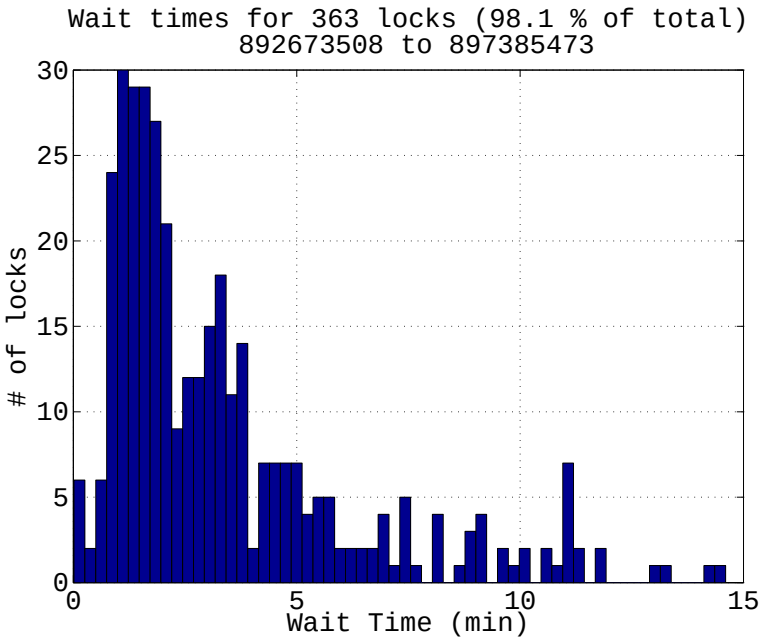

Figure 3.5: Histogram of waiting times to acquire initial control of five length degrees of freedom. Lock wait times longer than 15 minutes are excluded from the data.

DOF	**Control Signal**	**Trigger**
SRC	REFL166 I	REFL166 Q
PRC	REFL 33 I	SPOB
MICH	REFL 33 Q	SPOB
XARM	$1/\sqrt{TRX}$ − offset	TRX
YARM	$1/\sqrt{TRY}$ − offset	TRY

Table 3.1: Control signals and loop triggers for initial lock acquisition of the 40m detuned RSE interferometer. These are the control signals used to bring the interferometer from an initially uncontrolled state to state A. The output of the control system for each DOF is independently switched on/off according to the value of the signal in the *Trigger* column.

DOF	Initial Signal	$\Longrightarrow$	Final Signal
MICH	REFL 33Q	$\Longrightarrow$	AS DD
PRC	REFL 33I	$\Longrightarrow$	REFL DD
SRC	REFL 166I	$\Longrightarrow$	PO DD

Table 3.2: Hand off of Short DOFs.

resembles the final configuration, and making the transition at this stage simplifies the process of the bringing the arms into full resonance. Since the point reached in step A is one where both arm cavities are detuned from resonance in the same direction and by the same amount, there is effectively an offset in the CARM DOF. The rest of the lock acquisition process involves reducing and finally removing this CARM offset. The CARM and DARM signals are closely related to the single arm signals, and are calculated in a similar manner using the transmitted power from the arm cavities:

$$DARM_{DC} = \frac{TRX - TRY}{TRX + TRY} \tag{3.8}$$

$$CARM_{DC} = X_{DC} + Y_{DC} \tag{3.9}$$

The calculated signals can also be seen in the purple portion of Figure 3.10.

Step D: Hand off control of DARM

The $DARM_{DC}$ signal calculated from the arm cavity powers is a noisy signal and designed only for temporary use. Thus, at this earliest opportunity, we take advantage of the fact that there is no offset in the DARM degree of freedom, and transition control of DARM directly to its final design signal. This can be the RF DARM or a DC Readout DARM (based on the transmission of an OMC). Each of these has advantages and disadvantages. As the CARM offset is reduced during the remainder of the lock acquisition process, the RF DARM signal will undergo a shift in demodulation phase as the CARM

offset is reduced. This is because CARM offset is primarily held constant by keeping the arm cavities off resonance, and the phase of the fields reflected from the arm cavities rotate as they approach resonance (see Figure C.2). The two arms rotate in such a way that at the asymmetric port of the IFO, the field amplitudes continue to cancel, but the phase angle at which a field due to DARM motion would appear is rotating. This is shown schematically using a phasor diagram in Figure 3.5.2. The DC Readout DARM signal also undergoes changes as the CARM offset is reduced and the power in the IFO increases: the gain of the signal increases, and the DARM offset required for DC Readout changes if the setpoint in the DARM loop is determined by power transmitted through the OMC. If the setpoint is adjusted to keep the DARM offset the same, the increased power at the asymmetric port will cause the gain of any loops pertaining to controlling the OMC (in both length and alignment) to increase, and so some compensation will be required to keep these loops stable.

Step E: Hand off control of CARM to MCL

At this stage, the residual frequency noise of the laser is large enough to be problematic for maintaining control of the interferometer, in part because the signals used at this stage are more sensitive to laser frequency noise than the signals used at the operating point. To counter this, we begin the process of matching the laser frequency to the common arm length (CARM), using a servo system known as the Common Mode (CM) servo. The first step in engaging the CM servo is to take the error signal which senses the CARM DOF and feed it back to the Input Mode Cleaner length (MCL path). This ensures that the mode cleaner length and the common arm length share a common resonant frequency; as the laser frequency feedback is following the mode cleaner length, the laser frequency is now also matched to the common arm length, within the bandwidth of the MCL path ($\approx 100\,\mathrm{Hz}$).

Step F: Engage frequency path of CM servo

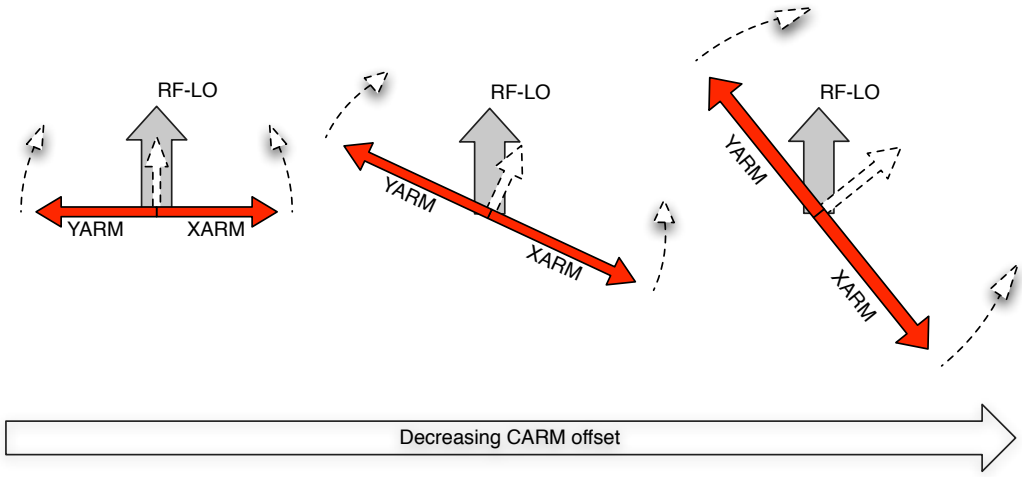

Figure 3.6: As the CARM offset is reduced, the arm cavities move closer to resonance, causing the phase of the reflected fields to rotate. Since the angle of the RF local oscillator is set by the demodulation phase, it does not rotate with the change in CARM offset. The dotted lines indicate arm cavity motion in a differential arm (DARM) mode.

Above $\approx 100\,\mathrm{Hz}$, the suspended mode cleaner provides a quiet reference for the laser frequency, and thus the laser frequency is altered to match the mode cleaner length. The feedback of the high-frequency path of the CM servo injects a signal into the error point of the mode cleaner servo, generating an additive offset (AO). The mode cleaner servo then acts to suppress the sum of its error signal and the AO, causing a mismatch of the laser frequency and the mode cleaner length. The laser frequency is matched to the common arm length, however, within the bandwidth of the CM servo (several kHz). Once a high enough bandwidth is achieved, the adaptive compensation discussed in 3.5.5 can be turned off. Because it is desirable to allow the frequency path (MCF-AO) to have a very high bandwidth, it is necessary to find an analog signal which has the appropriate properties (e.g., it is sensitive to the mismatch between the laser frequency and the CARM length, over a range of CARM offsets, with a somewhat stable frequency response). Calculated signals such as that used for length feedback to the ETMs ($CARM_{DC}$) cannot be used because the sampling rate of the digital control system is too low (16384 Hz). One signal which meets these requirements is the light-power level in the recycling cavity (known as PO_{DC}). Because the CARM DOF is offset from resonance, this signal is sensitive to the CARM-laser frequency mismatch. This signal is fed back to the laser frequency after AC coupling to the AO path of the CM servo. It is necessary to appropriately match the relative gains of the frequency and length paths in order to ensure servo stability at the crossover frequency.

Step G: Increase CM Servo bandwidth and reduce CARM offset

Once the bandwidth of the CM servo is significantly greater than the peak in the CARM optical response, the CARM offset can begin to be reduced. This increases the carrier light power circulating in the IFO, and so any control loop gains which are sensitive to the carrier power must be adjusted to keep the loops stable. This includes the CM servo, as the gain in the AO path

(sensed by PO_{DC}) will increase. The gain in the AO path can be reduced to compensate, or it can be set in step F such that there is enough headroom to accommodate the increase.

Step H: Hand off CARM to RF

Once the CARM offset has been reduced to the point where the buildup of power in the IFO is greater than half its final value, the standard, RF, PDH-style signals (such as in Figure 2.5 which are sensitive to CARM are within their linear range, and can be used for controlling CARM. Care must be taken at this stage to understand (through modeling) the frequency response of the DC and RF signals to ensure that they are commensurate. The MC-L feedback can be transitioned to an RF based signal digitally, while the MC-F feedback (which uses an analog signal) must be transitioned using some sort of cross-fade amplifier. These transitions should happen approximately simultaneously; the scripts used at the 40 m transition the digital portion half way, then transition the analog portion half way, finish the digital portion and then finish the digital portion. Only the digital path has gain at DC, so it is not difficult to add an offset to the RF error signal to ensure a smooth signal transition without actually changing the offset in CARM; because the analog path has no gain at DC, it does not require an offset.

Step I: Remove CARM offset

Once the CARM loop (including the CM servo) is using the RF signal, the remaining CARM offset is removed and the IFO is brought to its operating point. At this stage the controls system is ready to be transitioned to its final configuration. The electronic topology of the CM servo is described in section 3.5.7, and here it is noted that the final configuration implies that all signals for CARM are routed through the CM servo electronics (this includes the digital path, which is acquired digitally as an output of the electronics board). Since the CARM offset is zero, the analog error signal should also be zero, and high gain low frequency boost stages in the servo can be engaged.

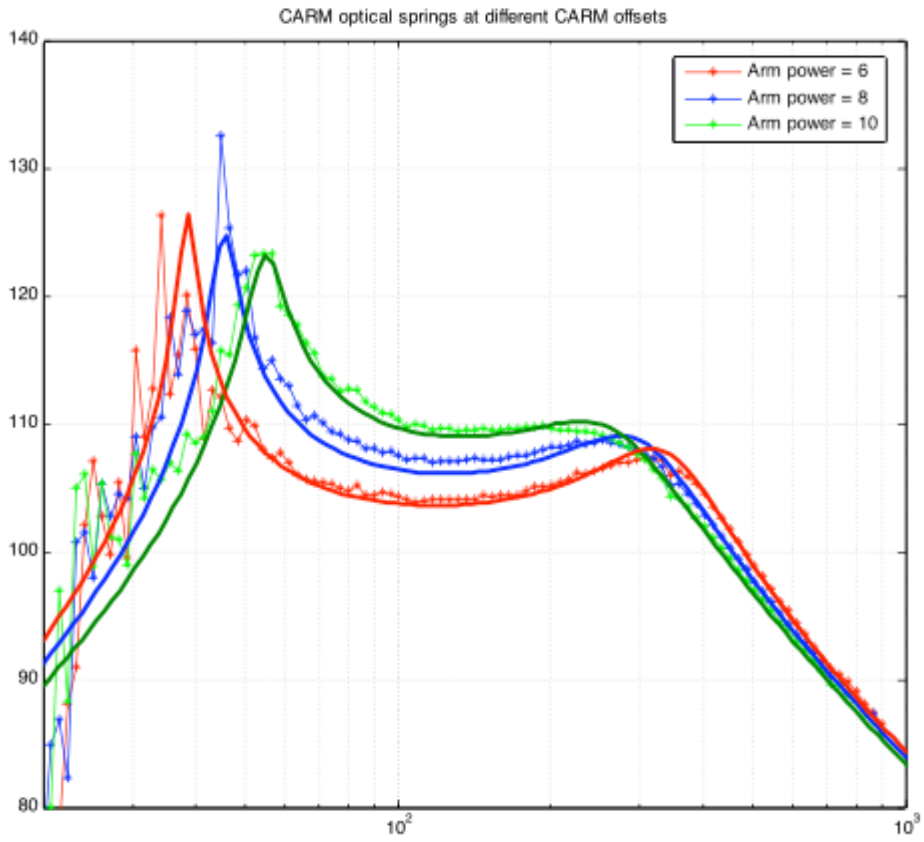

Figure 3.7: The optical response (magnitude only) of the CARM DOF at several CARM offsets. As the CARM offset is reduced and the circulating power increases, the peak in the optical response moves toward lower frequencies while the opto-mechanical spring resonance moves toward higher frequencies. Experimental data are shown in dots; the solid line is a simulation.

3.5.3 The spring and the anti-spring

For the DARM DOF, reversing the direction of the detuning in the SRC can change the optical response from one that is an optical spring to one that is an anti-spring. The anti-spring response has the same suppression of motion at low-frequencies, but has no resonant peak, and no phase increase at the resonant frequency. These differences are shown in Figure **??**. Detuning the CARM DOF in different directions results in similar behavior, with repercussions for control of the DOF.

The particular set of lock acquisition signals chosen for the procedure described in 3.5.2 link the springs in CARM and DARM. By examining the points in configuration space where both ARM transmitted powers are at the nominal locking point (one-half the buildup achieved in a single arm state) and writing down a signal matrix for sensing the lengths of the two ARMs, derived from the transmitted powers, we can infer which of those points might be reasonable choices for locking. As can be seen in Table 3.3, when the SRC is detuned to create a spring in DARM and the ARMs are detuned for a CARM anti-spring, the signal matrix is dominated by off-diagonal elements. This means that the procedure described in 3.5.2 links the CARM and DARM springs, so that both must be dealt with at once.

Switching the SRC detune from positive to negative can be accomplished experimentally in this setup by choosing whether the upper or lower f2 RF sideband resonates in the SRC. This also requires sign changes in the offset locking loops (to accommodate the fact that the CARM detune must also change sign) as well as any loops whose error signals are derived from the f2 sideband (such as DDM loops).

During development of the lock acquisition procedure (3.5.2), it was discovered that the two modes (spring and anti-spring) have different statistics for initial acquisition (such as in Figure **??**). More specifically, the MTTL is much longer for the spring mode than for the anti-spring mode, a discrepancy which remains unexplained. Modeling work has not confirmed the primary suspicion of higher-

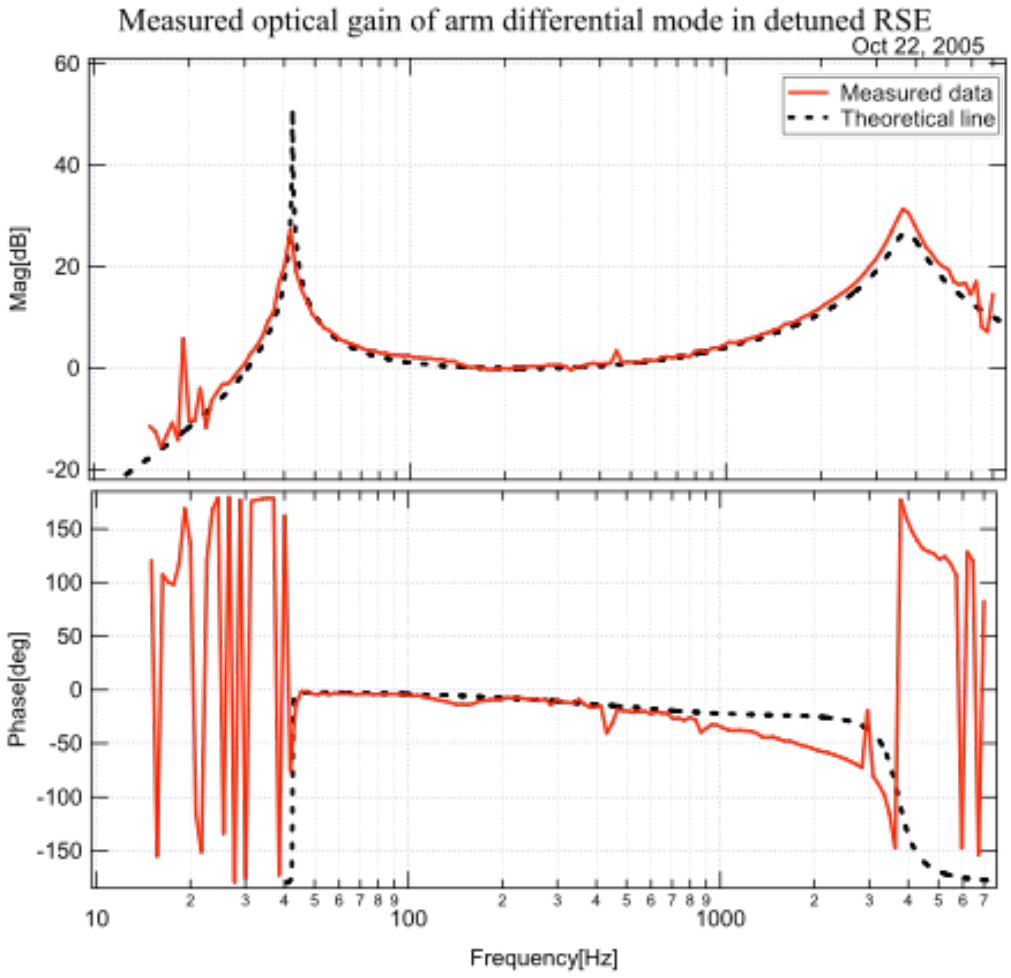

Figure 3.8: Data showing the optical response (in a Bode form) of the DARM degree of freedom in the nominal operating configuration. There is an opto-mechanical resonance near 40Hz and a purely optical resonance near 3.6kHz. A theoretical curve is also shown for comparison.

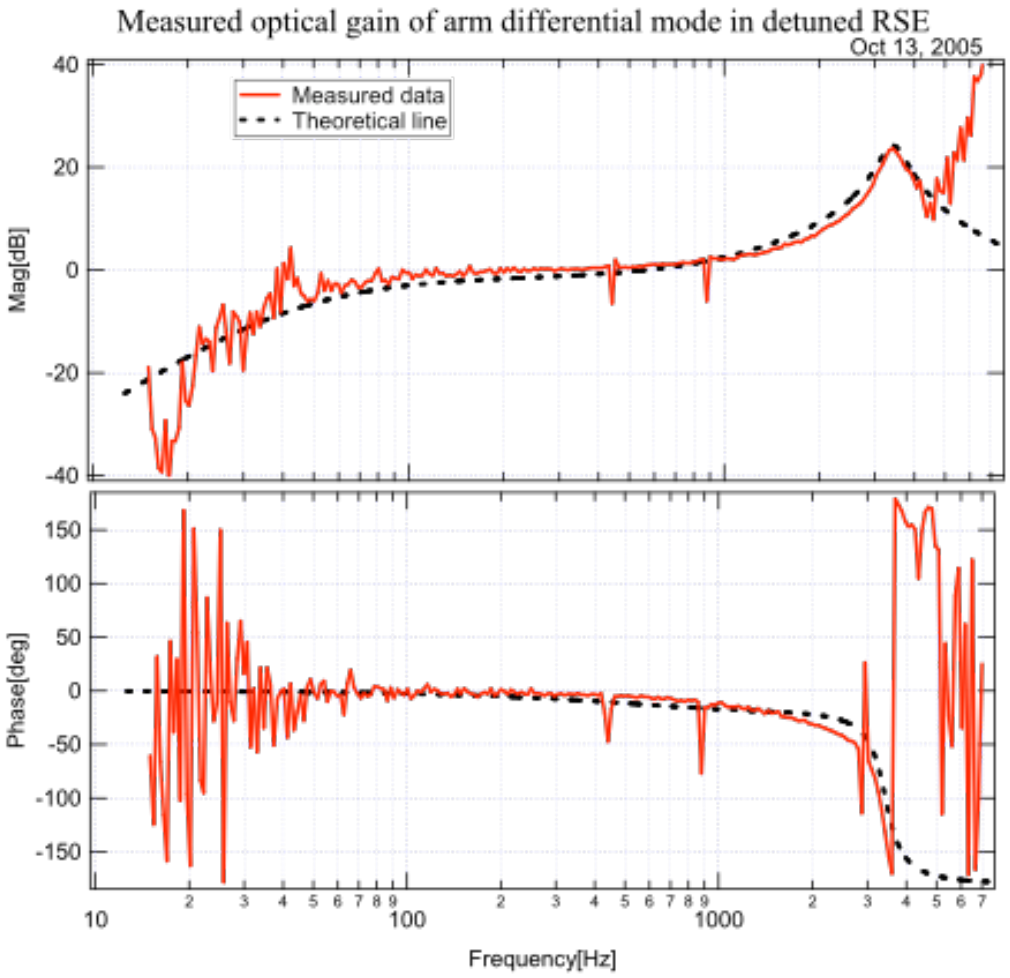

Figure 3.9: Data showing the optical response (in a Bode form) of the DARM degree of freedom in the anti-spring configuration. There is a purely optical resonance near 3.6kHz, and no opto-mechanical resonance. There is, however, a decrease in the response at low frequencies indicating an opto-mechanical anti-resonance. A theoretical curve is also shown for comparison.

		+detune		-detune	
		XARM	YARM	XARM	YARM
+CARM	TRX	2.8	5.3	4.7	3.1
	TRY	5.3	2.4	3.1	4.8
-CARM	TRX	4.6	3.2	2.7	5.3
	TRY	3.2	4.9	5.3	2.5

Table 3.3: Four sensing matrices for the individual arms (XARM and YARM) detected at the transmitted ports (DC). The numbers are in mWatts/pm, and the sensing matrices are at possible offset-lock points. Note that two matrices have larger diagonal elements, and two have larger off-diagonal elements.

order modes of either the carrier or RF sidebands resonating differentially in the arms or recycling cavities. signal matrix for all DOFs at two points?

3.5.4 Mode Healing

One predicted effect of signal recycling, discussed in [**?**], is mode healing. This occurs when undesirable junk light (such as higher order modes) is not resonant in the signal recycling cavity, masking the contrast defect.

3.5.5 Adaptive compensation filter: the moving zero

While the interferometer is locked with a CARM offset, it is effectively operating as a low-power double detuned interferometer. Referring to Figure 2.6, for DARM the detuning is in the short degree of freedom (l), while for CARM the detuning is in the long degree of freedom (L). The detune of the CARM degree of freedom creates a complex optical response which can impact the stability of the feedback loops which control the interferometer cavity lengths.

As the CARM offset is reduced, the detuning of the CARM degree of freedom changes, causing a change in the optical plant. This change takes the effect of a complex pole in the response function (the peak in the optical response) moving

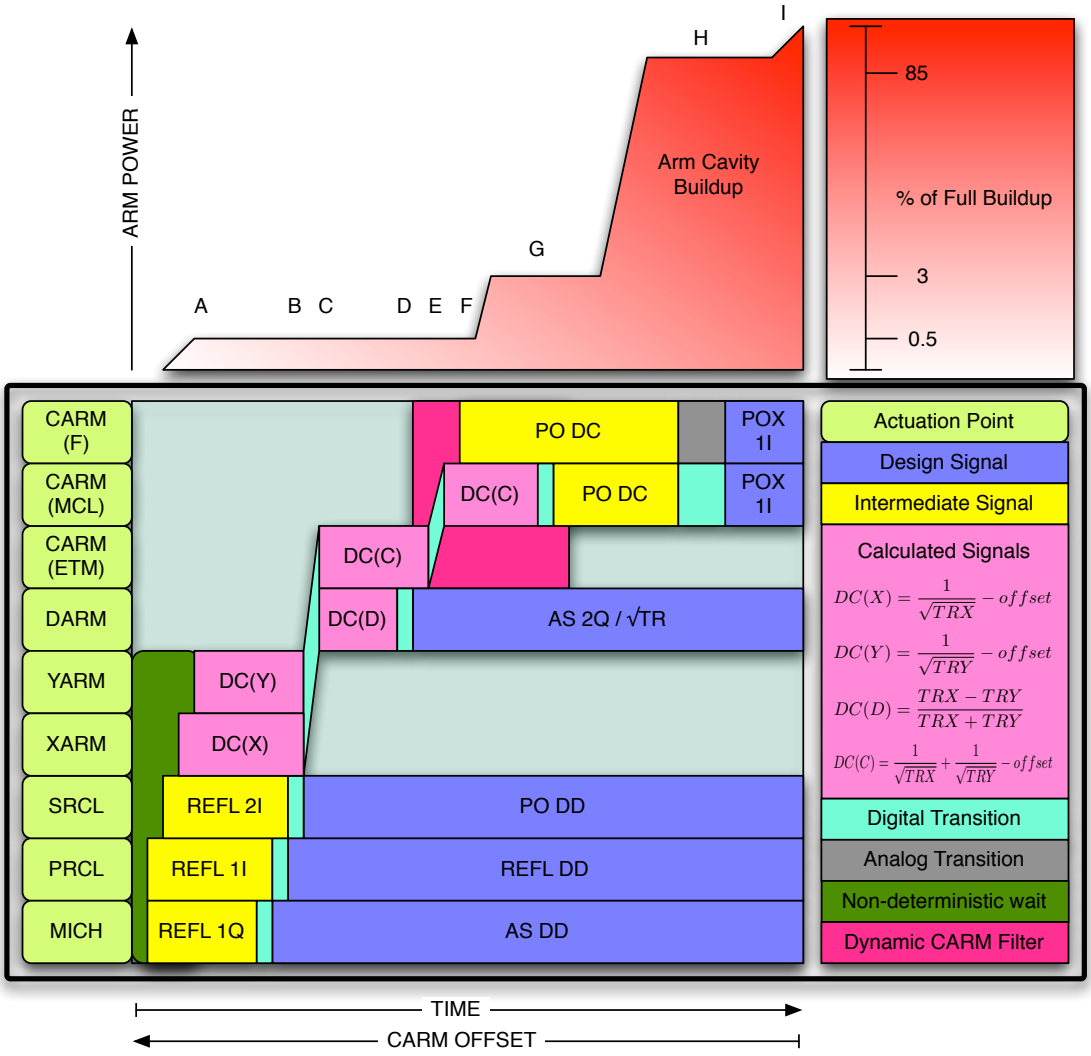

Figure 3.10: The sequence of error signal usage and transitions in the lock acquisition process developed for the 40 m RSE interferometer. The statistics of the non-deterministic stage (shown in green) can be inferred from Figure 3.5. The letters refer to the descriptions of the procedures in the text in sec. 3.5.2

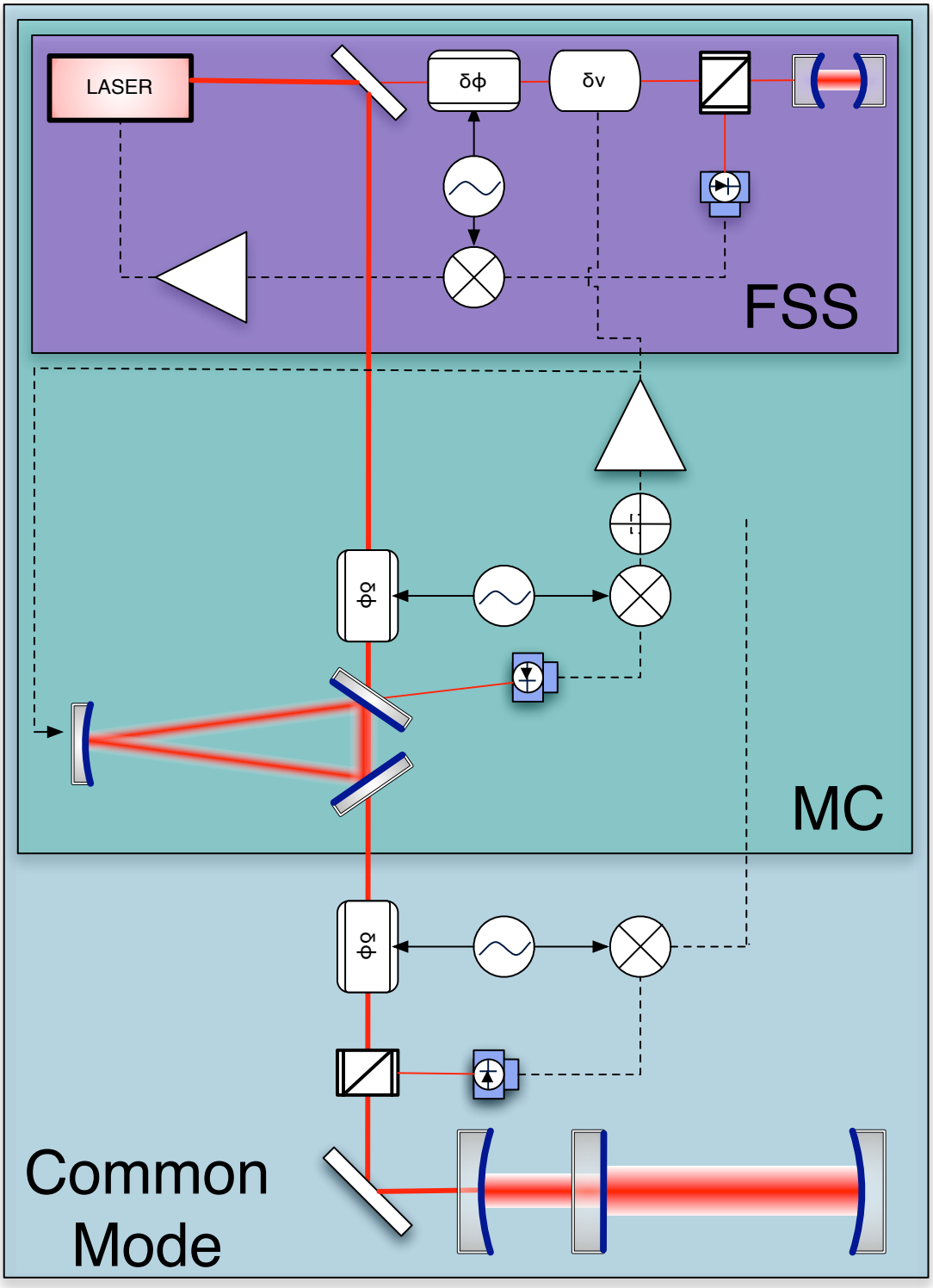

Figure 3.11: The laser frequency stabilization system.

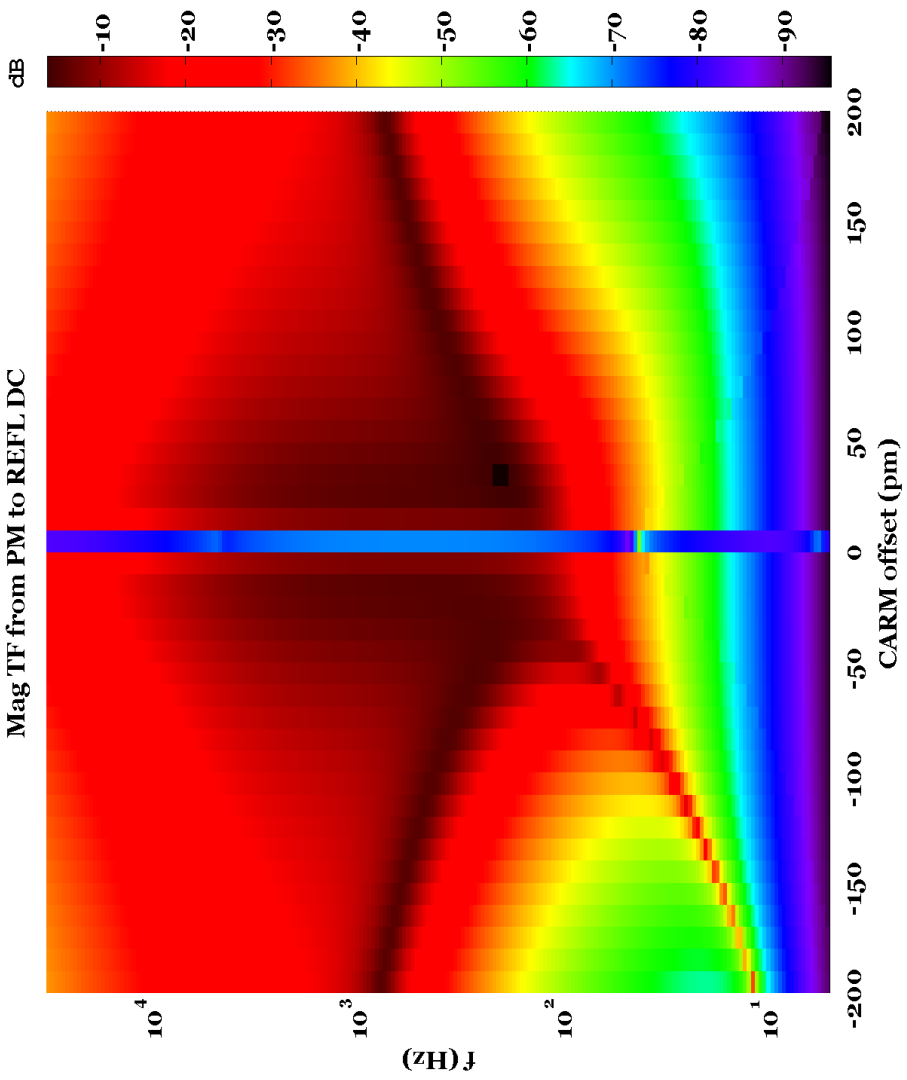

Figure 3.12: dB magnitude of the CARM (sensed at $REFL_{DC}$) open-loop opto-mechanical frequency response to input laser phase noise shown as a function of CARM offset.

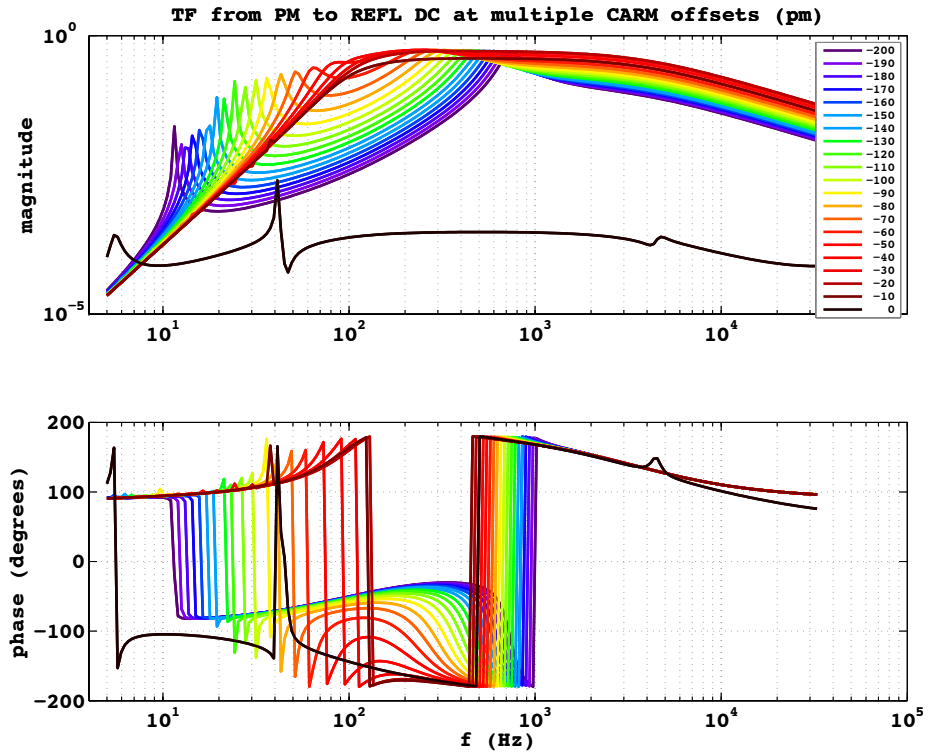

Figure 3.13: Bode plots of the opto-mechanical frequency response of $REFL_{DC}$ to input laser phase noise, at various CARM offsets. This selection shows a series of offsets which lead to spring-behavior in CARM; offsets from resonance in the other direction would exhibit anti-spring behavior. Some features, such as the ripple near 4kHz, are due to IFO imbalances which couple frequency noise into DARM, and DARM motion to $REFL_{DC}$.

Table 3.4: This table is basically just notes. Ignore it.

$$\text{format} = \begin{matrix} \text{TRX(x)} & \text{TRX(y)} \\ \text{TRY(x)} & \text{TRY(y)} \end{matrix}$$

SRCL detune is at 37.6 XARM at 1.8342e-10 : YARM at 1.3317e-10

$$\text{senseMatrix} = \begin{matrix} 0.0028 & 0.0053 \\ 0.0053 & 0.0024 \end{matrix}$$

SRCL detune is at 37.6 XARM at -1.5578e-10 : YARM at -1.5955e-10

$$\text{senseMatrix} = \begin{matrix} 0.0046 & 0.0032 \\ 0.0032 & 0.0049 \end{matrix}$$

SRCL detune is at -37.6 XARM at 1.495e-10 : YARM at 1.6583e-10

$$\text{senseMatrix} = \begin{matrix} 0.0047 & 0.0031 \\ 0.0031 & 0.0048 \end{matrix}$$

SRCL detune is at -37.6 XARM at -1.7839e-10 : YARM at -1.3819e-10

$$\text{senseMatrix} = \begin{matrix} 0.0027 & 0.0053 \\ 0.0053 & 0.0025 \end{matrix}$$

from a relatively high frequency (at $\approx 1\,\text{kHz}$) towards the on-resonance common mode coupled cavity pole (at $\approx 100\,\text{Hz}$). This particular sweep of frequencies carries this complex pole through the UGF of the CARM loop, creating an excess phase delay which causes the stability of the control loop to degrade. To prevent this, a digital filter which adapts to the changing response was implemented. This filter is composed of a flat path summed with a path rising like f^2. The flat path is gain-adjusted by being divided by current build-up of power in the arm cavities. Thus, as the power builds in the interferometer, this division compensates the increasing optical gain. The path which rises like f^2 is not gain compensated, however, and so as the power builds in the interferometer the crossover frequency of the f^0 path and the f^2 path moves downward in frequency along with the pole in the coupled cavity response. Figure 3.15 shows the action of this compensating filter with several transfer function measurements detailing the CARM cavity optical response at different CARM offsets along open-loop transfer functions which show the performance of the compensation filter.

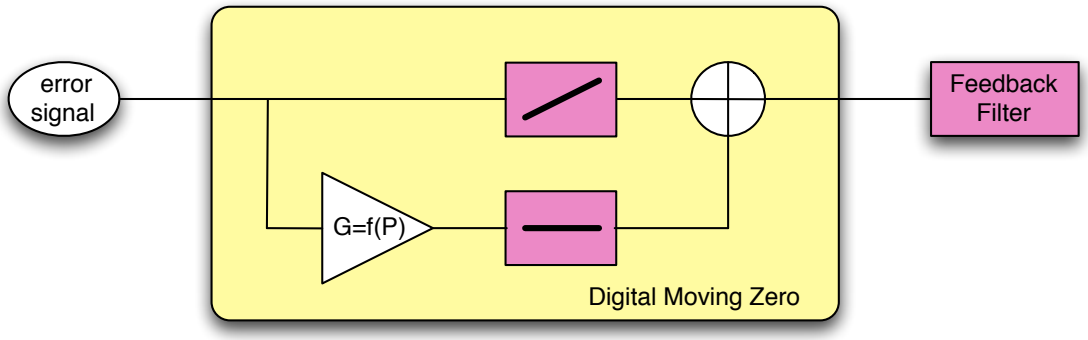

Figure 3.14: The topology of the compensation filter used in the CARM loop. The function $G(f)$ is $\sqrt{P_{tr}}$.

Relevance to Advanced LIGO

The basic philosophy of this technique will be employed in Advanced LIGO, although the details of the initial stage will differ. The current planned technique is described at the end of 3.6.

3.5.6 Scripting Tools

The lock acquisition procedure developed relies heavily on scripting tools to automate and coordinate repetitive and routine tasks. Figure 3.16 is a flow diagram of the sequence employed by the master locking script.

3.5.7 The Common Mode Servo

The Common Mode Servo is the final stage of frequency stabilization in the LIGO interferometers, described in this section because it plays a crucial role in the lock acquisition process developed at the 40 m.

3.6 Deterministic Locking

The long tail of the distribution of waiting times for acquiring initial lock shown in Figure 3.5 motivated attempts to develop an alternate lock acquisition scheme

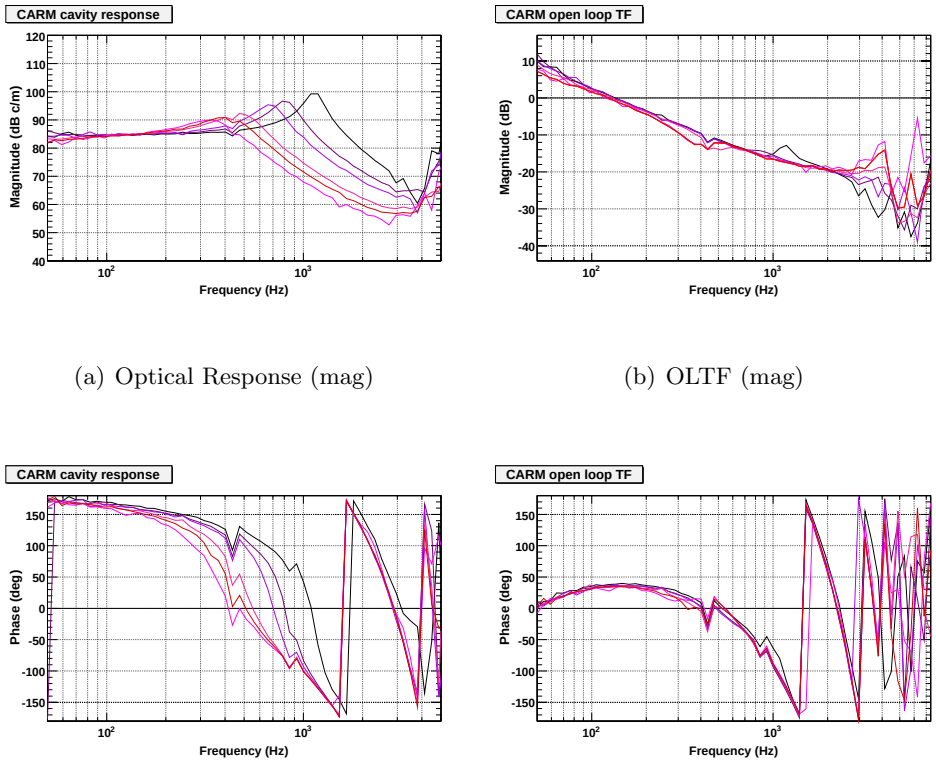

(a) Optical Response (mag)

(b) OLTF (mag)

(c) Optical Response (phase)

(d) OLTF (phase)

Figure 3.15: CARM cavity response and open loop transfer functions (near the UGF) for different CARM offsets. The dynamic cavity-pole compensation filter can be seen to be working, as the change in the open loop transfer function is much smaller than the changes in the optical response.

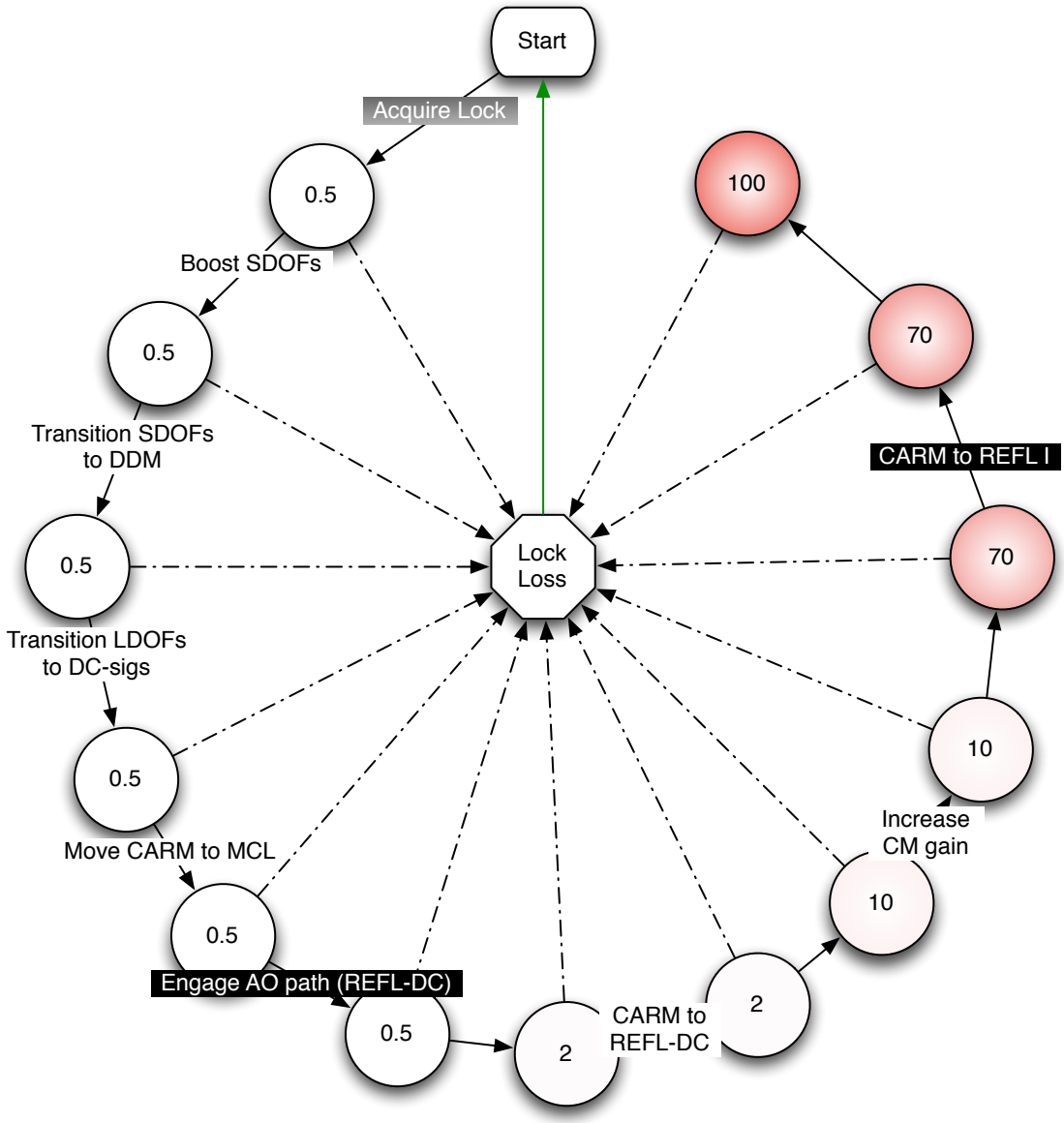

Figure 3.16: The flow of the primary locking script used for lock acquisition of the 40m detuned RSE interferometer. The circles show the build-up of circulating power in the interferometer arm cavities as a percentage of the full circulating power.

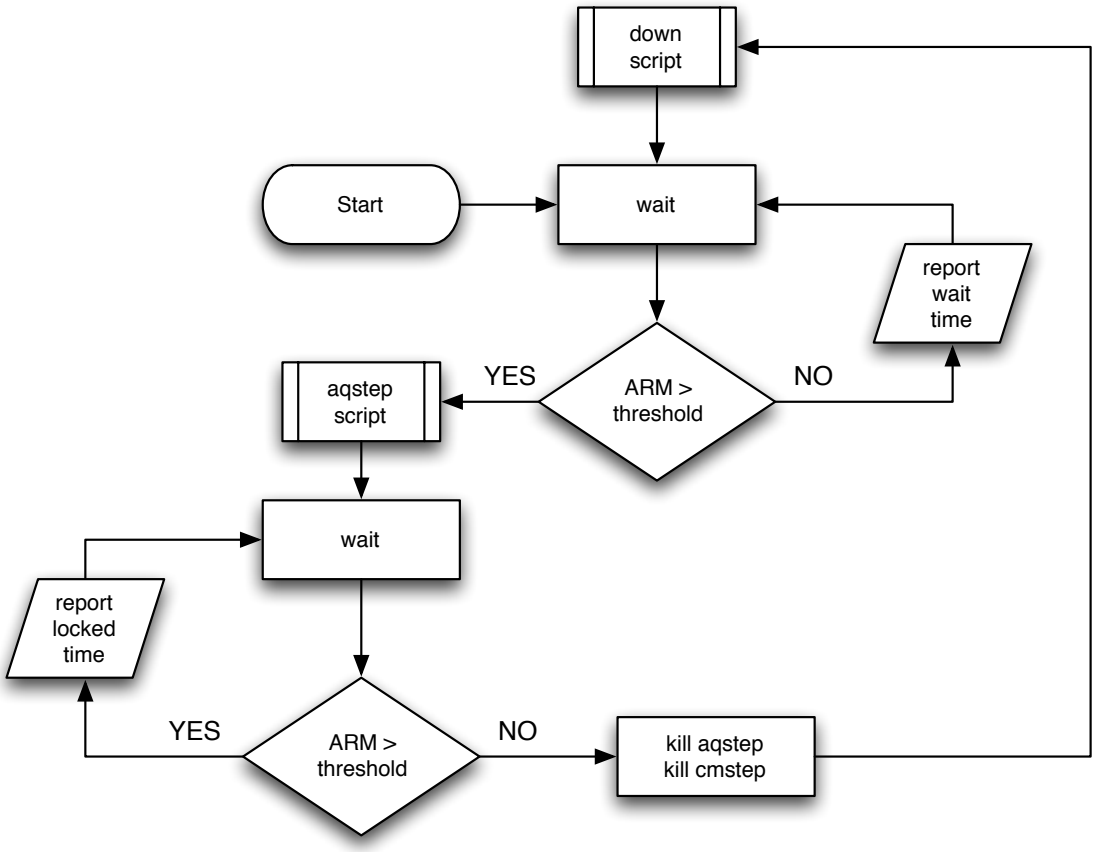

Figure 3.17: The flow of the main watch script used for locking.

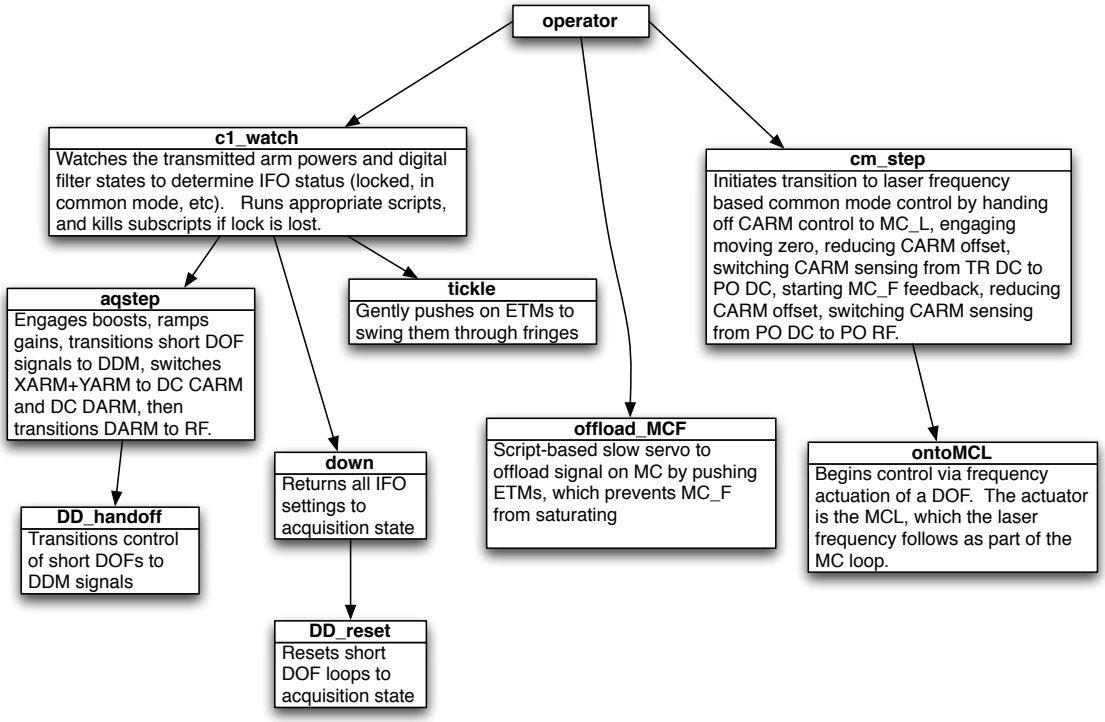

Figure 3.18: The hierarchcy of scripts used for automating lock acquisition of the 40 m.

which would be largely deterministic. Without continual, complete knowledge of the microscopic state of the interferometer, a truly deterministic lock acquisition process is impossible (and, moreover, unnecessary). *Deterministic locking* is thus a process which appears deterministic on human timescales–any statistical variations in process length are on the order of seconds rather than minutes. Such a process is a holy grail of lock acquisition, sought by gravitational wave interferometer scientists and commissioners the world over. It has many benefits, including reduced commissioning time (and consequently greater observation time), easier debugging of hardware and software, and much reduced frustration and boredom of detector operators. Some effort was expended at the 40 m to find a deterministic locking process for a power-recycled Fabry-Pérot Michelson interferometer (LIGO and Enhanced LIGO) configuration. Several promising candidates were explored, including mis-alignment techniques such as those employed in VIRGO (which involve mis-aligning certain optics, locking the resulting interferometer subset, and then re-aligning the optics in a controlled manner) and dynamic normalization techniques (which allow interferometer subsets to remain locked while uncontrolled DOFs swing through the available configuration space). These efforts were not pursued to completion because: a) the current LIGO lock acquisition process works well enough and b) the PRFPMI lock acquisition process developed for the 40 m (very similar to the process described in 3.5.2) already had the most desirable quality of a 'deterministic' procedure, as it very rarely took longer than 1 minute to complete the analogue of step A in 3.5.2.

Furthermore, significant effort was expended at the 40 m to find a deterministic locking process for a dual recycled Fabry-Pérot Michelson interferometer, as such a technique could be very useful for Advanced LIGO. No promising candidates were found, which serves to underline the added complexity in the controls plant introduced by the technique of signal recycling.

The failure to find a deterministic locking procedure for the 40 m has spurred a renewed effort at attempting yet more lock acquisition 'cheats'. These involve significant auxiliary hardware, such as secondary interferometers (operating in a

different color or polarization) which provide signals for lock acquisition. The goal is to be able to sense robustly a single DOF without interference from the other DOFs, and without causing interference to the other DOFs. Such an approach, which strives to reduce the dimensionality of the initial, statistical stage of lock acquisition, can greatly reduce the MTTL. A promising candidate strategy is described in the next section, and once key technologies are demonstrated it will be prototyped at the 40 m lab.

3.6.1 It's easy going green

One promising lock acquisition protocol would employ the philosophy described in this chapter (e.g., first locking the IFO away from the final operating point, and slowly bringing it towards resonance), with the assistance of a pair of auxiliary lasers. The advantages of the currently planned scheme include:

- Independent lasers allow independent sensing of two arms
- Independent damping of arm cavities
- Velocity damping greatly increases control
- green light allows for breaking degeneracy of acquisition & detection finesses
- green light allows significant isolation from disturbance by other degrees of freedom, also isolates the short DOFs from the arm cavities
- green light with the wedge allows excellent isolation from other degrees of freedom, and helps to isolate the arms from each other.

The primary difference between the proposed green-light based scheme and the scheme described in 3.5.2 involves replacing step A with a version which is deterministic in nature.

The 40 m experience has demonstrated that is not difficult to lock a 3 DOF system such as that which comprises a dual-recycled Michelson, provided there is an appropriate selection of signals and the recycling cavities are of sufficiently low

finesse, which is the case for the current Advanced LIGO design. In order to have an essentially deterministic locking scheme for Advanced LIGO, it is thus sufficient to improve the locking time of the arm cavities, which can be accomplished with the addition of some auxiliary hardware dedicated to lock acquisition.

Hardware augmentation for lock acquisition

The additional hardware required includes, for *each arm* of the interferometer:

- A 4-km optical fiber
- A system to cancel any phase noise introduced by such a fiber
- A Nd:YAG single-mode NPRO laser with fast frequency tuning (e.g., fitted with a PZT), and the equipment necessary to phase-lock it to another laser.
- A low-noise Nd:YAG frequency-doubling system (such as with a nonlinear crystal)
- Dichroic coatings for the ITMs (highly reflective for green) and ETMs (low reflectivity for green)

Envisioned lock acquisition procedure

For each arm, 1064 nm light from the PSL will be coupled into the 4-km optical fiber and sent to the end station. The fiber system will require a setup to cancel phase noise induced by the fiber, such as the system devised in [13]. At the end station, a secondary NPRO will be phase-locked (with some frequency offset ω_o) to the PSL light transmitted through the fiber. The phase-referenced light from this secondary NPRO will be frequency-doubled to 532 nm. This green light will be phase modulated, and injected into the arm cavity through the ETM. With the ITM having a highly reflective coating for green light, this system now forms a low-finesse, over coupled cavity, and a standard PDH based length sensing and control scheme can be easily applied. If the phase-locking loop has a high enough

bandwidth, the PDH error signal can be fed back to the error point of the phase-locking loop, and the frequency of the green light can be made to follow the length of the cavity; this fast actuator combined with a low-finesse cavity will make for tremendously simple lock acquisition. The feedback loop should only be limited by the range of the frequency actuator for the NPRO, which should be at least 10's of MHz. Such a range corresponds to many free-spectral ranges of the arm cavity. Simply reading off the frequency control signal necessary to keep the green light resonating in the cavity thus provides a linear measure of the length of the arm cavity (relative to the wavelength of the PSL) over many wavelengths. This signal can then be used to velocity damp the cavity with the test mass actuators until the cavity motion is significantly less than a linewidth.

Once the arm is under length control, it can be held stably at a point near the carrier resonance. With the arm lengths held such that they fluctuate much less than a fringe, they will not disturb the signals for the short DOFs (MICH, PRC, SRC), control of which can be easily acquired using the techniques described in 3.5.2.

Once control of the short DOFs has been achieved, the full IFO is under control, and techniques similar to those described in Step B and onward in 3.5.2 can be used to bring the IFO to the operating point. Alternatively, it may also be possible to use the green light sensing chain to control the arm cavities independently while the offset is reduced; this might be possible if the initial lock stage is done at low laser power, thus avoiding significant radiation pressure effects. Radiation pressure effects can also be avoided by appropriately locking the SRC away from its own nominal operating point (detuning it), and adjusting this offset in concert with the arm offsets to eliminate any optical spring in the DARM degree of freedom. Such a procedure is conceivable as the sensing scheme for the SRC in Advanced LIGO has been designed to allow the SRC to be operable at multiple detunings, and to be able to switch between these detunings in lock.

Advantages of this technique

With an understanding of the technique, the advantages relative to the procedure in Step A of 3.5.2 become apparent:

- **Fiber delivery**: of the PSL light allows rear injection into the arm cavities.
- **Using green light**: breaks the degeneracy of cavity finesse for lock acquisition and GW detection; highly reflective ITMs isolates arm cavities from flashing in the short DOFs; highly reflective ITM plus the optic wedge angle serves to isolate arm cavities from flashing in the other arm cavity.
- **A Secondary Laser**: which is phase locked (with an adjustable frequency offset) to the PSL light allows the laser to be independent tuned, and thus locked to the cavity (rather than vice versa). The control signal for this loop can be used to velocity damp the cavity, which eliminates the need to for actuators that can acquire lock before the cavity has swept through a single fringe, sidestepping the concerns outlined in 3.3.
- **Two Secondary Lasers**: allow the two arms to be locked independently, both with a frequency control technique followed by velocity damping. Moreover, independent signals for the two arms allows the choice of locking to any point in the 2D CARM + DARM configuration space.